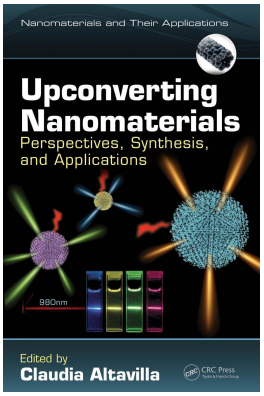

Upconverting Nanomaterials Perspectives, Synthesis, and Applications

Claudia Altavilla

Functionalization Aspects of Water Dispersible Upconversion Nanoparticles

Publication details
https://test.routledgehandbooks.com/doi/10.1201/9781315371535-6
Markus Buchner, Verena Muhr, Sandy-Franziska Himmelstoß, Thomas Hirsch
Published online on: 10 Oct 2016

4

Functionalization Aspects of Water Dispersible Upconversion Nanoparticles

Markus Buchner, Verena Muhr,
Sandy-Franziska Himmelstoß, and Thomas Hirsch

CONTENTS

4.1 Introduction

Upconversion nanoparticles (UCNPs)/nanomaterials have the unique property to absorb near-infrared (NIR) light which leads to an anti-*Stokes* emission from the ultraviolet (UV) over the visible to the NIR range (Zhang 2014). The NIR light is absorbed by sensitizer ions (e.g., Yb^{3+} and Nd^{3+}), and then transferred to so-called activator ions (e.g., Tm^{3+}, Er^{3+}, and Ho^{3+}) via a nonradiative, resonant energy transfer process. The lanthanide ions are preferably embedded in host lattices with low phonon energy and similar ionic radii to reduce nonradiative deactivation processes (Haase and Schäfer 2011; Suyver et al. 2006; Wang and Liu 2009). Fluorides combine low phonon energies (~300–400 cm^{-1}) with high chemical stability compared to other halide ions or oxide materials. The doping ratio of the sensitizer and activator ions is very critical, in order to generate highly fluorescent nanomaterials and to avoid self-quenching of the excited states. A $NaYF_4$ hexagonal host lattice

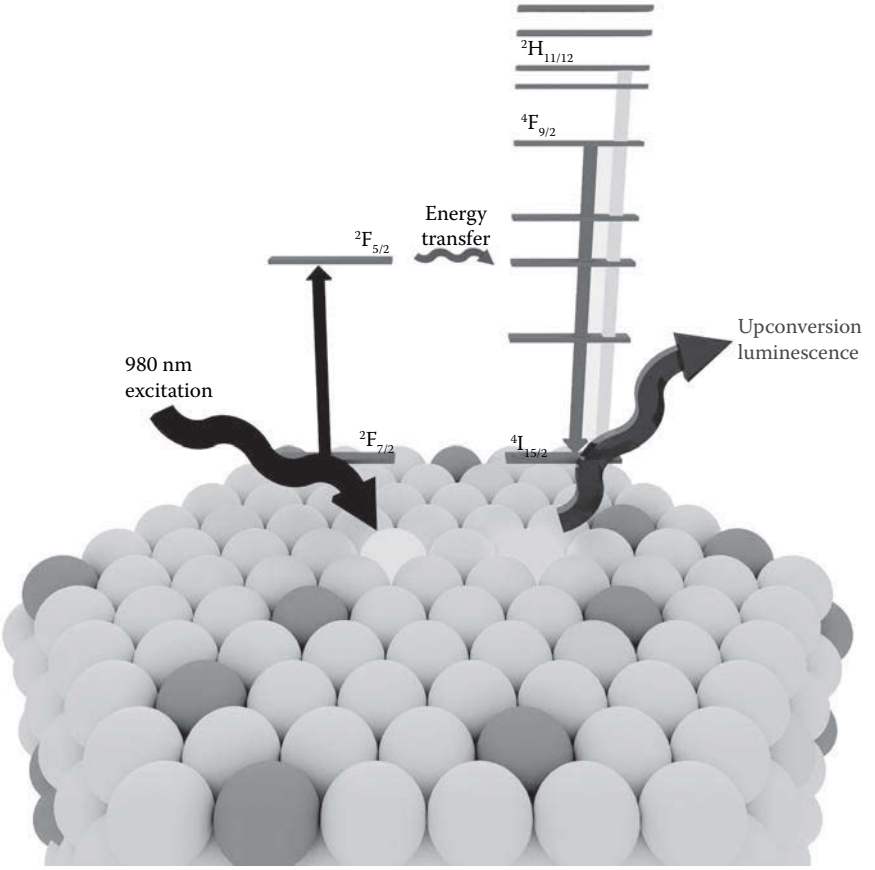

FIGURE 4.1
Hexagonal crystal lattice of $NaYF_4$ doped with 20% Yb ions and 2% Er ions. The Yb^{3+} ions are excited at 980 nm ($^2F_{7/2} \rightarrow {}^2F_{5/2}$) and transfer their energy to Er^{3+}, which can then either emit from the $^2H_{11/2}$ state (green emission) or the $^4F_{9/2}$ state after internal relaxation (red emission).

doped with Yb^{3+} and Er^{3+} ions and a simplified overview of the energy transfers inside the crystal is depicted in Figure 4.1.

The use of conventional fluorescent dyes in bioassays, biosensors, and imaging has been well established, but suffers from several drawbacks, such as high background fluorescence in biological matrices, photobleaching, small *Stokes* shifts, and short luminescence lifetimes. These disadvantages can be circumvented by the replacement of the dyes by UCNPs. The NIR excitation within the so-called optical window of biological material allows for deep tissue penetration without triggering autofluorescence of the matrix and reduced light scattering, leading to significantly higher signal-to-noise ratios. Beneficial properties, like high photostability, narrow

emission bands, long luminescence lifetimes, and low cytotoxicity, additionally qualify UCNPs for their use in the design of biosensing applications. Both homogenous and heterogeneous assays have been developed, facing different challenges when dealing with the optimization of the surface modification process regarding stability, sensitivity, and selectivity. Nucleic acids, proteins, and fluorescent organic dyes represent the most popular signal molecules for detection schemes using UCNPs.

4.2 Synthesis of UCNPs

The three main strategies for the synthesis of UCNPs are the thermolysis, the Ostwald ripening, and the hydrothermal strategy (Chen et al. 2014; Zhou et al. 2012). The hydrothermal strategy is usually performed in autoclaves with Teflon inserts. The precursors are mixed with surfactants like ethylenediaminetetraacetic acid (EDTA) or polyethylenimine. Hydrothermal syntheses typically have reaction times from 5 up to 24 h under high-pressure and temperatures up to 200°C (Wang et al. 2012). The diameter of the nanoparticles is in the range of 100–500 nm. It is extremely difficult to obtain smaller particles, especially diameters of about 20 nm, which is important for biological applications. The size distribution of the synthesized particles has been improved over the last years, resulting in almost monodisperse UCNPs. Another drawback is that the progress of the reaction cannot be controlled and the synthesis of uniform core–shell particles has not been realized via the hydrothermal strategy so far. The main advantage of the hydrothermal synthesis is the preparation of directly water dispersible nanoparticles.

In contrast, particles produced by thermal decomposition are not water dispersible after the synthesis (Boyer et al. 2006, 2007). The surface of the nanocrystal needs to be stabilized with organic surfactants. The most commonly used organic surfactants are oleate, oleylamine, and trioctylphosphine oxide. However, this method is superior regarding particle-size distributions and crystallinity.

The Ostwald ripening strategy relies on the fact that the growth of larger particles is energetically favored compared to smaller nanoparticles (Johnson et al. 2012; Rinkel et al. 2014). The synthesis is carried out in high boiling solvents (e.g., oleic acid and octadecene). First, lanthanide–surfactant complexes are formed as precursors at room temperature. In the next step, the precursors are heated up to approximately 300°C to grow the upconversion nanocrystals by Ostwald ripening. The advantages of the method are the narrow size distribution of the monodisperse nanoparticles, the purity in the crystal phase, and their enhanced optical properties. Wilhelm et al. (2015) showed that the progress of the reaction can be monitored by laser excitation allowing also a rough estimation of the size of the nanoparticles. Furthermore,

the synthesis of uniform core–shell nanoparticles can be achieved by the Ostwald ripening method. Wang and Liu (2014) summarized the synthesis of core–shell nanoparticles for multicolor imaging. Moreover, Wang et al. (2010) showed that the luminescent properties of small nanoparticles (<20 nm) increase dramatically by the surface passivation effect when growing a nondoped shell consisting of $NaGdF_4$ around Yb^{3+} and Tm^{3+}-doped $NaGdF_4$ core particles. Jayakumar et al. (2014) reported new strategies to shift the excitation wavelength of the UCNPs from 980 to 808 nm by incorporating Nd^{3+} ions in core–shell nanoparticles. In comparison with the excitation wavelength at 980 nm, water absorption is minimized under 808 nm laser excitation, yielding bright, luminescent nanoparticles in aqueous systems after successful surface modification. At the same time, the water heating effect caused by the 980 nm excitation is avoided, which is favorable for biological samples.

One drawback of the Ostwald ripening method is the hydrophobic character of the nanoparticles, which requests further surface modification for bioanalytical applications.

4.3 Surface Modifications of Hydrophobic UCNPs

The development of increasingly advanced, reproducible, and controllable synthesis protocols for efficient UCNPs resulted in interesting possibilities for the investigation of novel, powerful biosensing applications. The most efficient way to synthesize small, monodisperse UCNPs up to date is the Ostwald ripening method (Muhr et al. 2014). As mentioned before, the particles are covered with surfactants like oleic acid or oleylamine. The polar headgroup of the surfactants points toward the surface of the nanoparticles and coordinates the metal ions at the surface of the nanoparticles. The hydrophobic tails point outwards and restrict the colloidal stability of the nanoparticles to organic solvents like chloroform or cyclohexane. Consequently, the need for effective surface modification strategies to transfer hydrophobic nanocrystals into aqueous media is increased. Over the years, a variety of methods to render the particles water dispersible have been developed. The most common and effective strategies can be categorized into three main groups: amphiphilic coatings, silica shell formation, and ligand exchange. These three methods are shown in Figure 4.2 and are described as follows.

4.3.1 Amphiphilic Coatings

One straightforward and very powerful technique to warrant water dispersibility is the formation of an additional layer on top of oleate-capped UCNPs via the deposition of amphiphilic molecules. Their long alkyl

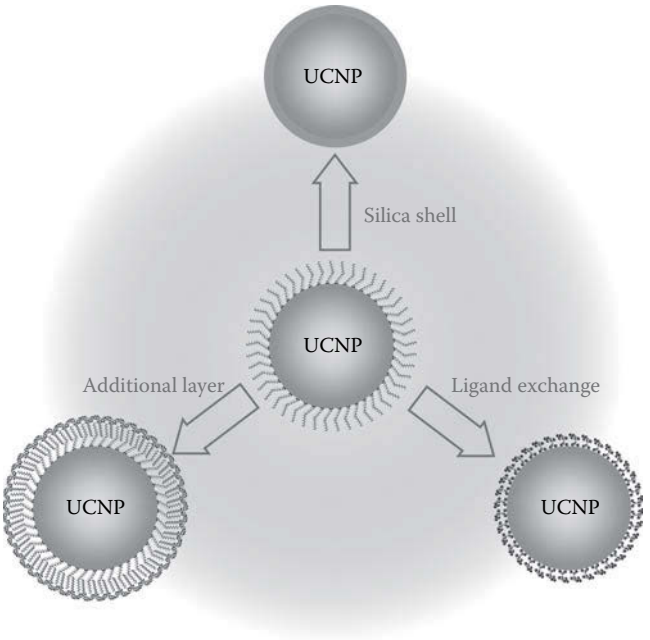

FIGURE 4.2
Overview of surface modification methods for transferring hydrophobic UCNPs into hydrophilic media by ligand exchange, additional layer deposition, and silica shell formation.

chains are able to intercalate between the hydrophobic oleate molecules based on van-der-Waals (vdW) interactions, thus forming a bilayer around the particle surface. However, the maximum length of the alkyl chain leading to a successful surface coating is limited by the length of the oleate itself. If the chain length exceeds the length of the oleate, the vdW interaction becomes too weak to stabilize the bilayer. The hydrophilic head groups of the amphiphiles are directed toward the solvent, which consequently renders the particles dispersible in aqueous media. The choice of the head group provides a simple way to alter and adjust the resulting surface charge according to the desired application. This first charged layer on the particle surface also enables the possibility for layer-by-layer coatings, that is, the deposition of several layers with alternating charges. However, the head groups of the amphiphilic molecules do not only ensure water dispersibility. They also represent functional groups allowing for the coupling of the coated UCNPs to receptor molecules or the attachment of, for example, dyes and stabilizing molecules.

In this context, phospholipids represent a group of frequently used amphiphiles for the surface modification of UCNPs. Phospholipids are commercially available with a great variety of different head groups, which ensures flexibility regarding the final surface coating. Particles modified with

phospholipids are generally taken up by cells quite easily, and exhibit low cytotoxicity and biocompatibility, which is usually achieved by the addition of poly(ethylene glycol) (PEG) units (Nam et al. 2011; Park et al. 2009).

However, phospholipids are quite challenging regarding their synthesis and consequently expensive. Therefore, surface modification using much less-expensive surfactants has also been investigated. For example, TWEEN-80 (Ren et al. 2012) and several long-chain alkylammonium derived surfactants (Liang et al. 2012) have been successfully applied as amphiphilic surface coatings on UCNPs. Nevertheless, the colloidal stability of the resulting particles in aqueous systems was not as good as of the phospholipid-coated ones.

The use of amphiphilic polymers instead of small surfactants or phospholipids is one approach to further increase colloidal stability (Pellegrino et al. 2004). As these polymers contain a large number of hydrophobic alkyl chains per molecule, they are better stabilized against ligand detachment by a chelating effect. Poly(maleic anhydride-*alt*-1-octadecene) (PMAO) is the most widely used representative for the group of amphiphilic polymers (Li et al. 2014; Wang et al. 2011). UCNPs coated with PMAO display excellent colloidal stability in buffers over a wide pH range and in cell culture media for weeks (Jiang et al. 2012).

4.3.2 Encapsulation with Silica

The deposition of a silica shell on UCNPs is one of the most common techniques to achieve water dispersibility and to introduce functional groups to the particle surface. Hydrophobic UCNPs can be coated with a uniform layer of silica based on a reverse microemulsion method, which involves the polymerization of silicate precursors in the presence of a surfactant that forms and stabilizes the reverse microemulsion. The precursor tetraethyl orthosilicate (TEOS) and the nonionic surfactant Igepal CO-520 are most often used. Usually, a small amount of ammonia is added in order to keep the concentration of silicic acid above the nucleation concentration, which leads to the steady growth of a uniform silica shell. The thickness of the resulting shell depends on the amount of both precursor material and surfactant present during the shell growth phase. Particles encapsulated within silica are dispersible in water, are taken up by cells fast, and display low cytotoxicity (Jalil and Zhang 2008).

Yet, the colloidal stability of such UCNPs@SiO_2 in aqueous dispersions is quite poor, which leads to their aggregation and consequently precipitation within hours (Idris et al. 2012; Wang et al. 2009a). This problem arises through the centrifugation of the particles during purification. After centrifugation, it is often completely impossible to redisperse the particles in water. One solution for this problem is the stabilization of the silica-coated UCNPs by an increased surface charge in order to reduce the aggregation tendency (Bagwe et al. 2006). The desired high surface charge can be achieved by the

introduction of negatively or positively charged functional groups on the silica surface. This can be done either by silanizing the already coated particles or by the addition of functional organosilanes during the polymerization process, for example, carboxyethylsilanetriol (F. Liu et al. 2013) or aminopropyltrimethoxysilane (Wang et al. 2009b). By optimizing the surface chemistry on UCNPs@SiO_2, it was possible to stabilize them in various kinds of buffers, including phosphate buffer and cell culture media.

It is also possible to synthesize mesoporous silica shells around nanoparticles. They exhibit an extremely large surface area with tunable pore sizes. Molecules can be easily trapped inside the pores of this material. These properties make them especially interesting for applications in drug delivery (J. Liu et al. 2013; K. Li et al. 2015). Another possibility is to load the mesoporous shell with dyes or receptor molecules that otherwise would not be able to penetrate the cell membrane (C. Li et al. 2013).

4.3.3 Ligand Exchange

Surface modification by ligand exchange is a third possibility to obtain water dispersible UCNPs. Here, the original ligand, for example, oleate is replaced either by small hydrophilic molecules or polymers. In a typical one-step procedure, the hydrophobic UCNPs are treated with a solution containing an excess of the desired new surface ligand at elevated temperatures for several hours. Usually, the protocol has to be adjusted for every single ligand regarding optimum reaction conditions. Commonly used hydrophilic molecules for the modification of nanoparticles via ligand exchange are citrate, poly(acrylic acid) (PAA) (J. Wang et al. 2014), poly(vinylpyrrolidone) (Johnson et al. 2010), and PEGylated compounds (Tong et al. 2015).

Other protocols for ligand exchange are based on two-step processes. The first step is the complete removal of the hydrophobic ligand oleate. One possibility to strip off the oleate is the addition of strong acids, for example, HCl (Bogdan et al. 2011). The oleate is protonated by the acid and thus released from the particle surface, leading to the generation of more or less ligand free particles. Another way to remove the oleate is the treatment with nitrosyl tetrafluoroborate ($NOBF_4$) (Dong et al. 2011). In this case, BF_4^- ions provide an electrostatic stabilization of the ligand free particles, consequently preventing particle aggregation during the exchange process, as it is usually the case for most one-step methods. In the second step, the desired new capping molecule is attached. After isolation and purification, the bare nanoparticles are stirred together with a solution containing the new surface ligand for passivation of the nanocrystal surface. Here, usually heating and protective gas are not required, and reaction times are considerably shorter compared to the more common one-step procedures (Ni et al. 2014; Y.-F. Wang et al. 2013).

In general, ligand exchange is an extremely versatile technique, as there are almost no limitations to their applicability. The only requirement for the new ligand molecule is the presence of a functional group capable of

coordinating to the surface of the UCNPs. Negatively charged groups, such as carboxylates, sulfonates, phosphonates, and readily available free electron pairs, like in amino groups, fulfill this requirement. Thus, almost every molecule containing at least one of the mentioned functional groups can be successfully applied for the ligand exchange process. In contrast to surface modification by amphiphilic coatings and silica shells, ligand exchange provides a way to attach the new ligand directly to the surface of the UCNPs. The distance between the particle and ligand is thus minimized, which is, for example, especially important for applications relying on energy transfer processes between UCNPs and organic dyes immobilized on their surface.

When working with multifunctional molecules, the concentration of the UCNPs and the desired ligand has to be carefully adjusted in order to prevent cross-linking between several particles. Nevertheless, crosslinking and thus aggregation of the particles during the ligand exchange cannot be prevented completely. Another drawback of this method is the poor colloidal stability of the water dispersible UCNPs in solutions with high ionic strength and especially in phosphate buffer. Here, the use of strongly coordinating phosphates as new capping molecules provides increased stability in buffered systems (Ma et al. 2014; Zhao et al. 2014). Also, the application of water-soluble polymers instead of small molecules as the new ligand, improves the temporal colloidal stability in these systems due to the higher stability of the polymer against its detachment from the particle surface. Additional to the water dispersibility, a great number of possible functions suitable for further coupling are provided at the surface, since not every single functional group of one polymer chain is directed toward the particle. The first charged polymer layer can also function as first charged layer for successive layer-by-layer coatings (C. Wang et al. 2013).

To introduce biofunctionality to UCNPs, the surface of the water dispersible particles needs to be further engineered. The next chapters give an overview of strategies for coupling proteins, nucleic acids, and dyes to UCNPs as well as their bioanalytical applications.

4.4 Protein Conjugation

Antibodies, a special class of proteins and best known for their unique recognition ability, have been attached to UCNPs, for example, for the establishment of an immune sandwich assay of carcinoembryonic antigen (CEA) (Y. Li et al. 2015). The CEA in test samples was first captured with magnetic beads (MBs) coated with anti-CEA antibodies. After washing steps assisted by magnetic separation, the addition of PAA-capped UCNP with anti-CEA antibodies led to the formation of sandwich structures on the MBs connected by the CEA. Excess UCNP composites were removed and the luminescence

emission of the UCNPs was recorded, resulting in a linear behavior for concentrations of the CEA between 0.05 and 20 ng mL^{-1}. The anti-CEA coated UCNPs exhibited good stability in 4-(2-hydroxyethyl)-1-piperazineethanesulfonic acid (HEPES) buffer.

Ong et al. (2014) proved the high photostability of the UCNPs in comparison with the green fluorescent protein (GFP). First, they performed a ligand exchange to remove oleate from the surface of the UCNPs and introduce citrate as a new ligand. As example, an anti-*E. coli* antibody was bound via classical 1-ethyl-3-(3-dimethylaminopropyl)carbodiimide (EDC) chemistry to the citrate-coated nanoparticles. After binding to *E. coli*, the halftime of GFP was determined to 75 s by fluorescence imaging, while the signal of the UCNPs stayed nearly constant over 30 min. Special focus was put on the colloidal stability and monodispersity of the nanoparticles. After the binding of the antibody, the hydrodynamic diameter of the particles increased about 200 nm with a low PdI of 0.162. Consequently, also with reference to the transmission electron microscopy (TEM) images, agglomeration was not critical. The binding of the particles to the *E. coli* cells showed only vulnerability against the growth medium lysogeny broth.

Binding of antibodies to silica-modified UCNPs generates conjugates of UCNPs and antibodies colloidally stable in phosphate buffer. Zhang et al. (2007) embedded a photosensitizer into silica shells around UCNPs and an anti-MUC1/episialin antibody was bound to the amino functionalized silica shell through cyanogen bromide.

Qiao et al. (2015) presented a very elegant technique to bind antibodies to the surface of UCNPs. They removed oleic acid from the core–shell $NaGdF_4$:Yb,Er @$NaGdF_4$ particles by heating to 50°C and adding an asymmetric PEG containing a maleimide group at one end and a diphosphate on the other end. The disulfide groups of a monoclonal antibody were reduced with tris(2-carboxyethyl)phosphine hydrochloride and the obtained thiol groups were bound to the maleimide groups on the surface of the nanoparticles by click reaction. Due to the coordinating phosphate groups on the surface, the modified particles were even stable in phosphate buffered saline (PBS) and can be used for a large area of applications.

Wang et al. (2009b) grew a silica shell around $NaYF_4$:Yb,Er nanoparticles using the classical *Stöber* synthesis. In a second step, 3-aminopropyltrimethoxysilane was used to functionalize the surface of the nanoparticles with amino groups and a rabbit anti-CEA8 antibody was bound to the nanoparticles via EDC chemistry.

The unique recognition properties and the high catalytic activities of enzymes are commercially used in several bioassays and sensors. In combination with UCNPs, the most critical point is the crosslinking of the particles and enzymes after immobilization to the surface of the nanoparticles. Crosslinking and as a result changes in the tertiary structure lead to lower catalytic activities. Gao et al. (2015) immobilized a caged protein kinase (PKA) on the surface of UCNPs, which can be activated by NIR light inside

cells. $NaYF_4$:Yb,Tm nanoparticles were synthesized in high boiling solvents and a silica shell was formed by a reverse microemulsion method by adding Igepal CO-520 and TEOS. Considering the corresponding TEM images and dynamic light scattering (DLS) measurements, the particles were partially aggregated. The caged protein was bound to the surface of the silica-coated nanoparticles via electrostatic interactions. With the Bradford assay, the amount of the protein in the supernatant was calculated to roughly 4.5 nmol of PKA per 1 mg nanoparticle. The thiol groups of the enzymes were caged with o-nitrobenzyl bromide. After NIR excitation of the UCNPs, o-nitrobenzyl bromide was cleaved from the active center as shown in Figure 4.3 and the enzyme was used for the monitoring of intracellular signal transduction.

Chien et al. (2013) used a similar method to target cancer cells by creating a photoresponsive molecule with folic acid and o-nitrobenzyl bromide. The photosensitive protecting group was cleaved from folic acid by NIR excitation. Wang et al. (2015) developed a successful detection method for hyaluronidase. Hyaluronic acid-capped $NaYF_4$:Yb,Er UCNPs were bound with EDC chemistry to poly(m-phenylenediamine) nanospheres. Due to the electron rich properties of the nanospheres, the green emission of the UCNPs was fully quenched. In presence of hyaluronidase, the UCNPs were released from the surface and the green luminescence of the particles was recovered.

In relationship with UCNPs, enzymes are very often used in combination with organic molecules and dyes, which are able to absorb the emitted upconversion luminescence. Wilhelm et al. (2014) showed that they could monitor the production of nicotinamide adenine dinucleotide (NADH) and flavin adenine dinucleotide (FAD) due to the spectral overlap with Yb^{3+}, Tm^{3+}-doped core–shell $NaYF_4$ nanoparticles.

Wilhelm et al. (2013) presented a general approach for biomodification of silica-coated UCNPs with proteins. First, a silica shell was formed by the reverse microemulsion method. Subsequently, the silica surface was

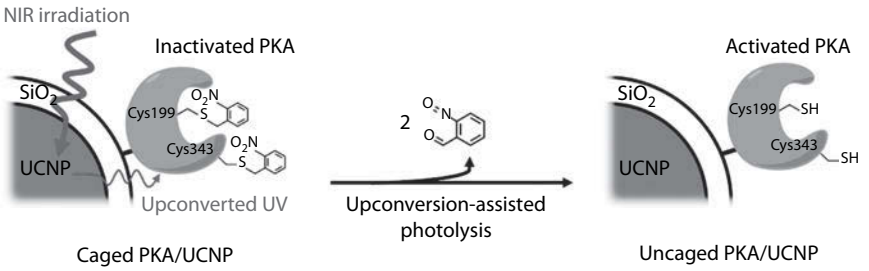

FIGURE 4.3
Caged PKA/UCNP complex design and the process of upconversion-assisted PKA uncaging. (Reprinted with permission from Gao, H.-D., P. Thanasekaran, C.-W. Chiang et al. 2015. Construction of a near-infrared-activatable enzyme platform to remotely trigger intracellular signal transduction using an upconversion nanoparticle. *ACS Nano* 9, 7041–7051. Copyright 2015 American Chemical Society.)

modified with a silane-PEG2000-N-hydroxysuccinimide (NHS) for biocompatibility and reactivity toward amino groups. The functionalized particles were conjugated to streptavidin-coated MBs demonstrating the high reactivity toward proteins.

Min et al. (2014) used photoactivation through UCNPs to release a platinum antitumor drug. An amino functionalized silica shell was formed around $NaYF_4$:Yb,Tm particles, using TEOS and (3-aminopropyl)triethoxysilane. Mal-dPEG™$_6$-NHS was used as a linker to bind trans, trans, trans-$[Pt(N_3)_2(OH)_2(py)_2]$ to a thiol group of a peptide linker to the silica surface of the particles. By NIR excitation, the cell toxic Pt(IV) complex was cleaved from the peptide linker by the blue Tm^{3+} emission. The triggered cell death was monitored by an energy transfer of Tm^{3+}-doped particles to Cy5™, also attached to the surface of the UCNPs. The energy transfer was first blocked by the quencher Qsy21, which was cleaved from the surface of the nanoparticles by caspase-3 by entering apoptosis.

4.5 Conjugation to Nucleic Acids

Nucleic acids play an irreplaceable role in the detection of pathogens and toxins. Countless DNA hybridization assays and aptasensors have been developed for quantification and imaging purposes *in vitro* and *in vivo*. While common colorimetric and fluorescence-based techniques usually suffer from high background signals, photobleaching or cytotoxicity, the application of UCNPs as fluorescent labels circumvents these drawbacks due to their NIR excitation, large anti-*Stokes* shifted emission, and exceptional photostability. The conjugation of nucleotides to the surface of UCNPs is the most critical step during the design of a sensor or imaging platform. Extensive crosslinking due to multifunctional ligands, control over the amount of receptors on the particle surface, and the stability of the modified UCNPs in buffers and cell culture media represent the most important factors to consider when facing the decision on the type of surface modification strategy.

Ligand exchange is by far the most popular technique to functionalize UCNPs with nucleic acids due to its abundant versatility and simplicity. Either the oligonucleotide itself is used for the ligand replacement and is directly bound to the particle surface, or water-soluble molecules or polymers containing functional groups are used as new surface ligands to which subsequently the nucleotides can be coupled. The direct attachment of the nucleic acids represents the most straightforward approach, as it does not require any precedent chemical modification of the DNA for coupling chemistry. The nucleotides are hereby efficiently bound to the surface of the UCNPs via their strongly coordinating phosphate moieties. Due to the high binding affinity of those phosphate groups on the particle surface, the

DNA-coated UCNPs exhibit excellent colloidal stability in phosphate buffer and cell culture media.

For example, DNA was directly attached to $NaYF_4$:Yb,Tm@$NaYF_4$ nanoparticles aimed to determine S1 endonuclease activity (Huang et al. 2015a). The UCNPs were first modified with DNA by stirring the oligonucleotide together with oleate-capped particles in a two-phase system consisting of water and cyclohexane. The oleate was completely replaced by the ssDNA and the UCNPs were transferred into the aqueous phase. These DNA-modified UCNPs were able to adsorb to the surface of graphene oxide due to π-stacking interactions. Graphene oxide is capable of quenching the luminescence of the UCNPs adsorbed on its surface. When the DNA on the UCNPs was cleaved by the addition of the endonuclease, the particles were released from the graphene oxide. Consequently, the quenching effect decreased, leading to stronger emission intensities of the UCNPs. By monitoring the increase of the luminescence intensity, S1 nuclease activity of 1×10^{-4} units mL^{-1} was detected selectively.

The same group used the identical modification strategy with DNA via direct exchange at the liquid–liquid interface for the development of a detection scheme for Hg^{2+} ions based on nonradiative electron/hole recombination annihilation through an effective electron transfer process (Huang et al. 2015b). The Hg^{2+} ions could be selectively detected in a dynamic range between 10 nM and 10 μM.

In another example, the oleate ligand of $NaYF_4$:Yb,Er UCNPs was directly replaced by ssDNA by vigorous stirring in a water–chloroform mixture, leading to the formation of water dispersible DNA-coated particles (L.-L. Li et al. 2013). The UCNP–DNA conjugate showed stability against ligand detachment after hybridization with the complementary DNA strand labeled with gold nanoparticles (AuNPs), illustrating their potential for applications in hybridization assays as shown in Figure 4.4. The possibility for cell imaging and cancer cell targeting was also demonstrated by the hybridization of the UCNP–DNA conjugates with Cy3 labeled complementary DNA or the immobilization of a nucleolin-specific aptamer on the UCNPs, respectively. The DNA-modified UCNPs showed exceptional transfection capabilities, making them an excellent material of choice for targeted bioimaging and gene delivery.

Despite its simplicity, the direct attachment of the nucleotides is prone to several problems. Although the high binding affinity of the phosphate groups to the surface of the UCNPs leads to colloidal stability, the odds are that several UCNPs are crosslinked due the presence of multiple phosphate functionalities on one DNA strand. This can cause the formation of large networks and aggregates that are no longer colloidally stable in dispersion and precipitate. There is also the risk that the DNA strands wrap themselves around the particle. The nucleotides are then no longer available for any hybridization with the target DNA, which then leads to reduced detection sensitivities.

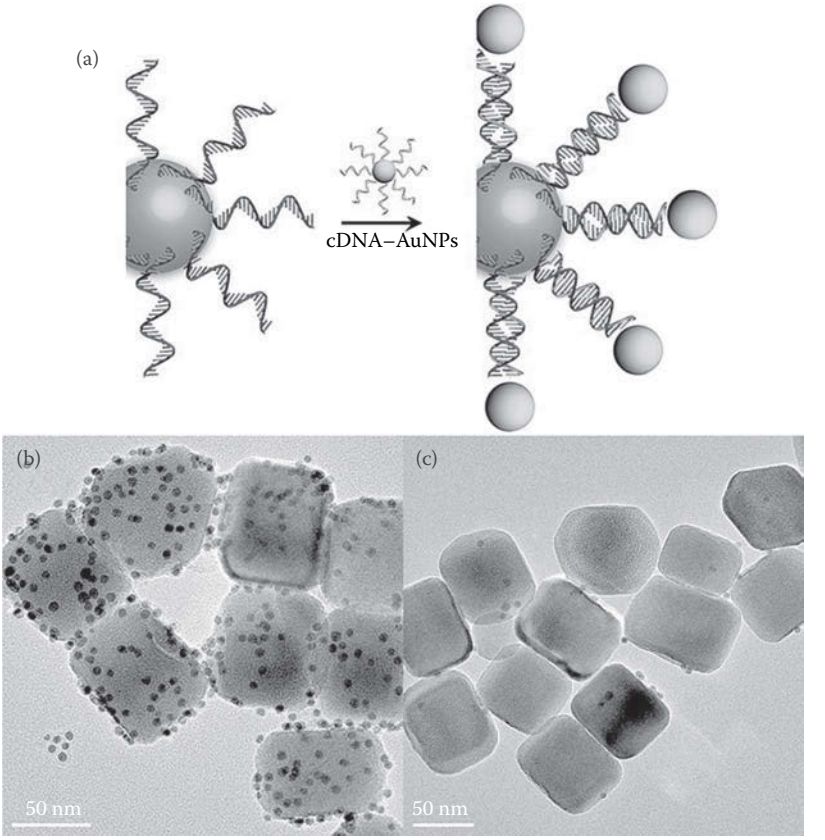

FIGURE 4.4
(a) DNA-directed assembly of UCNPs and AuNPs. TEM images of T30-UCNPs assembled with AuNPs bearing (b) complementary DNA and (c) noncomplementary DNA. (Reprinted with permission from Li et al. 2013. Copyright 2013 American Chemical Society.)

This can be prevented by the use of linker molecules, which are first bound to the UCNPs by ligand exchange, followed by the coupling of nucleic acids in a second step. These linker molecules have to carry both, a functional group with high binding affinity to the surface of the UCNPs and carboxyl or amino moieties, for binding to correspondingly functionalized nucleic acids.

Small bifunctional molecules such as dimercaptosuccinic acid (Lan et al. 2015) and aminoethanephosphonic acid (Song et al. 2012) have been successfully used as linkers for the conjugation of DNA to UCNPs. After ligand exchange, the carboxyl and amino groups were activated with EDC/NHS or glutaraldehyde, respectively, in order to couple amino-functionalized DNA or avidin for subsequent attachment of biotin-modified DNA. Both conjugates were used for the design of energy transfer-based sensors for the detection of either microRNA or adenosine triphosphate (ATP).

Ligands containing single binding sites, like in the two examples mentioned above, are prone to detachment from the particle surface, particularly in buffers containing phosphate ions and high ionic strength in general. In contrast to that, the use of polymers comprising multiple binding sites provides better stabilization against ligand detachment and functional groups for subsequent bioconjugation. The most frequently applied polymer is PAA.

In order to conjugate hydrophobic $NaYF_4$:Yb,Er,Mn to ssDNA for the detection of *staphylococcal enterotoxin B* (SEB), the oleate was first replaced by PAA in a one-step ligand exchange process in diethylene glycol (S. Wu et al. 2013). The ssDNA was then attached to the PAA-coated particles via carbodiimide chemistry and afterwards hybridized with the complementary DNA strand labeled with the dark quencher BHQ_3. After the hybridization, no red luminescence from the Mn^{2+}-doped UCNPs occurred. The degradation of the DNA by treatment with SEB led to the release of the quencher and consequently an increase of the UCNP luminescence intensity proportional to the SEB concentration. The detection limit for SEB was determined to be as low as 0.3 pg mL^{-1} with high reproducibility and specificity.

A similar approach was used for the development of a method for the simultaneous detection of three pathogenic bacteria (S. Wu et al. 2014). Three different kinds of UCNPs were synthesized, each exhibiting a different emission wavelength in the blue (Tm), green (Ho), or red (Er, Mn) region. After exchanging the oleate with PAA in a one-step procedure in diethylene glycol, three different amino-functionalized DNA strands (aptamers) were attached to the carboxyl groups on the particle surface by activation with EDC/NHS. Magnetic nanoparticles (MNPs) were modified equally with the complementary DNA, and both particle types were connected by hybridization. When the target bacteria were present, the UCNP-aptamer conjugates preferably bound to the specific binding sites on the bacteria. The luminescence signal of the remaining UCNP–MNPs conjugates was evaluated after magnetic separation from the UCNPs bound to the bacteria. The more bacteria present, the lower was the residual upconversion luminescence intensity. The whole assay principle is displayed in Figure 4.5. The limits of detection for the three target bacteria were found to be between 10 and 25 cfu mL^{-1}.

Ligand exchange is also popular for the design of heterogeneous immunoassays and aptasensors. Ulrich Krull et al. have especially performed pioneering research in the area of solid phase-based assay formats.

They performed a hybridization assay based on energy transfer on cellulose paper (Zhou et al. 2014). The UCNPs were first coated with citrate via a two-step ligand exchange assisted by HCl, conjugated to streptavidin by carbodiimide activation, and suspended in borate buffer. The modified UCNPs were immobilized on cellulose paper in small spots and biotin-tagged probe

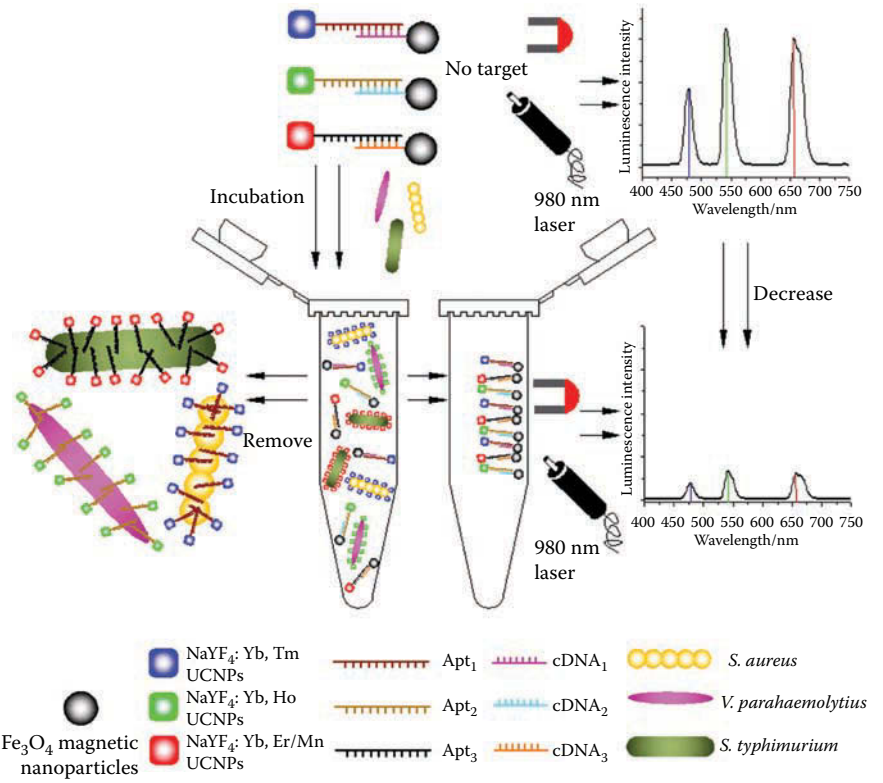

FIGURE 4.5
Schematic illustration of the multiplexed luminescence bioassay based on aptamer-modified UCNPs for the simultaneous detection of various pathogenic bacteria. (Reprinted with permission from Wu et al. 2014. Copyright 2013 American Chemical Society.)

DNA was bound to the particles on the paper. After treatment with the Cy3-labeled target DNA solution, the luminescence intensity of the UCNPs was read out using an epifluorescence microscope. The more target DNA was added, the lower was the remaining luminescence intensity due to a more efficient energy transfer from the UCNPs to the bound Cy3, achieving an limit of detection (LOD) of 34 fmol of target DNA. With this assay format, it was even possible to reliably discriminate between the complementary DNA and one base pair mismatch targets.

In another approach, UCNPs bound on cover slips have been used for the detection of thrombin (Doughan et al. 2014). $NaYF_4$:Yb,Tm@$NaYF_4$ UCNPs were first modified with o-phosphorylethanolamine (PEA) by ligand exchange. These particles were then immobilized on aldehyde-functionalized cover slips forming a densely packed layer on the glass surface. The immobilized nanoparticles showed stability against washing at three different pH

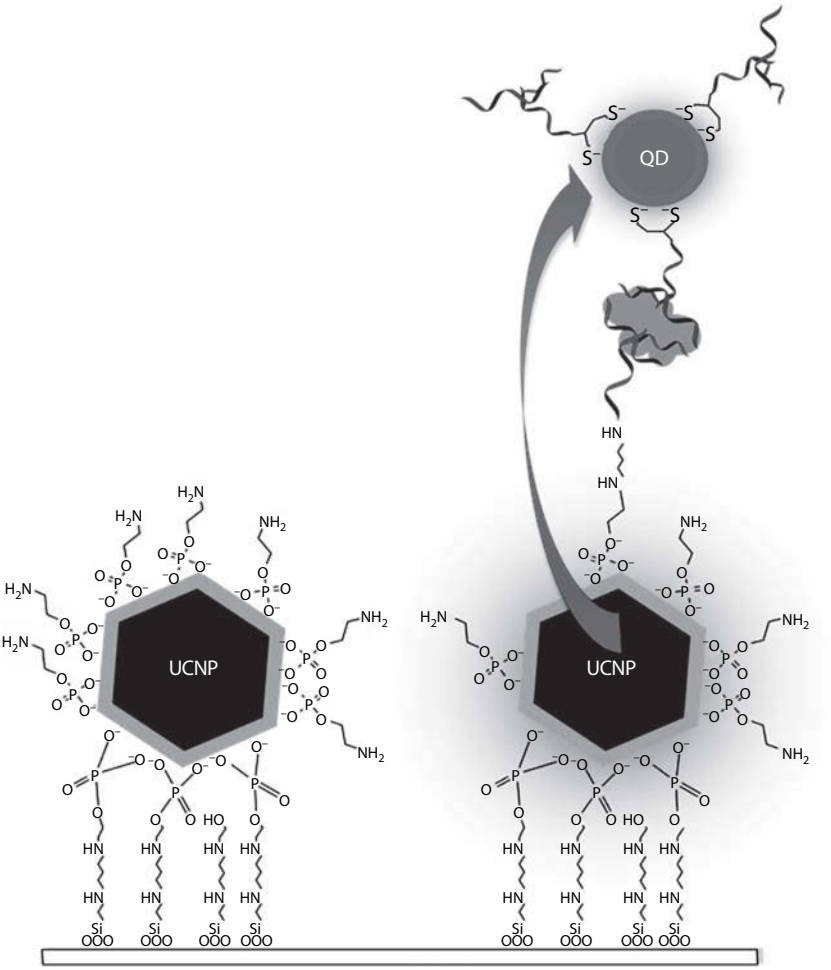

FIGURE 4.6
Schematic showing immobilization of PEA-UCNP on aldehyde-functionalized cover slip and use in the detection of thrombin using two different thrombin-specific aptamers. (Reprinted with permission from Doughan, S., Y. Han, U. Uddayasankar, and U. J. Krull. 2014. Solid-phase covalent immobilization of upconverting nanoparticles for biosensing by luminescence resonance energy transfer. *ACS Appl. Mater. Inter.* 6, 14061–14068. Copyright 2014 American Chemical Society.)

values of 5.5, 7.4, and 8.5; no leakage was observed. Next, a thrombin-specific aptamer was conjugated to the UCNPs on the cover slips. After thrombin was captured, quantum dots (QDs) also tagged with a thrombin-specific aptamer were added. The resulting conjugate is depicted in Figure 4.6. The overlap of the UCNP emission and the QD absorption led to a reduction of the observed upconversion luminescence intensity of the UCNPs and to an

increase of the luminescence of the QDs. It was possible to detect down to 230 fmol thrombin by evaluation of the intensity ratios of all involved emission peaks.

Generally, UCNP–DNA conjugates obtained via ligand replacement are prone to aggregation during the exchange process caused by crosslinking between multiple particles and control over the loading capacity of the nucleic acids on the particle surface is rather difficult.

The formation of a bilayer on top of oleate-coated UCNPs with the help of amphiphilic molecules is much less commonly used to prepare particles for conjugation to nucleic acids, but does not suffer from the same drawbacks as the ligand exchange strategy mentioned earlier.

In one example, such UCNPs were used for the determination of human immunodeficiency virus (HIV) antibodies (Y.-M. Wu et al. 2014). Here, the particles were simultaneously modified with two different phospholipids in order to control the receptor density on the particle surface. One lipid carried a PEG chain imparting increased colloidal stability and biocompatibility, the other one an HIV specific aptamer. The luminescence of these water dispersible UCNPs was completely quenched by GOx due to π-stacking interactions. In the presence of HIV, the aptamer immobilized on the particles specifically bound to the target virus, which prevented the adsorption to the GOx and led to linearly increasing luminescence intensity for HIV concentrations between 5 and 150 nM in diluted human blood serum.

Coating with phospholipids enables efficient control over surface loading with the DNA probe in one step by adjusting the ratio of two or more different phospholipids used for the surface modification, while at the same time imparting excellent colloidal stability in a variety of buffers. However, phospholipids are expensive and their synthesis and purification is fairly elaborate.

A second scarcely employed strategy for the immobilization of nucleotides to UCNPs is the prevenient growth of a functional silica shell suitable for bioconjugation.

For the design of a DNA sensor, the polymerization of TEOS around the particles in a reverse microemulsion was followed by silanization with 3-aminopropyl triethoxysilane, resulting in amino-functionalized $NaYF_4$:Yb,Er@SiO_2 (Alonso-Cristobal et al. 2015). The amino groups were then reacted with succinic anhydride and the resulting carboxyl moieties were used for the attachment of amino-functionalized ssDNA via carbodiimide coupling, as illustrated in Figure 4.7. Due to electrostatic repulsion between the charged functional groups, the reaction steps did not cause aggregation, precipitation of the particles, and no crosslinking was observed. The hybridization of the target DNA to the modified UCNPs was monitored by the evaluation of the quenching efficiency of GOx caused by π–π interactions with the remaining ssDNA on the particles. The LOD of this sensor setup was calculated to be 5 nM.

FIGURE 4.7
Schematic illustration of the chemical route for the functionalization of UCNPs@SiO_2 nanoparticles. (Reprinted with permission from Alonso-Cristobal, P., P. Vilela, A. El-Sagheer et al. 2015. Highly sensitive DNA sensor based on upconversion nanoparticles and graphene oxide. *ACS Appl. Mater. Inter.* 7, 12422–12429. Copyright 2015 American Chemical Society.)

4.6 Conjugation to Dyes

Fluorescent dyes are the most important tools for cellular imaging, sensing of intracellular parameters, and bioassays. Yet, many applications are limited by photobleaching and low signal-to-noise ratios caused by strong scattering of UV light, high autofluorescence, and unspecific binding. NIR excitable UCNPs can act as nanocarriers for those established dyes and eliminate these shortcomings by the design of conjugates relying on energy transfer mechanisms between the particles and the respective dyes. All applications share the necessity to select dyes that feature an overlap of their absorption spectrum with any emission band of the UCNPs. With this requirement in mind, numerous sensing schemes based on Förster resonance energy transfer (FRET) and inner filter effects have been reported. Almost as many different surface modification strategies for the attachment of fluorescent dyes to the particles have been described, all of which vary regarding stability, surface loading, distance between donor and acceptor, and sensitivity. All these parameters have to be carefully evaluated in respect to the final application before choosing one method.

Ligand exchange facilitates the attachment of dyes directly to the surface of UCNPs, which is especially favorable for efficient FRET processes due to the minimization of the distance between the donor–acceptor pair. In respect to applications in biological systems, this method only works for dyes which are water soluble and carry at least one functional group capable of binding to the surface of the UCNPs. Consequently, the colloidal stability in aqueous media solely depends on the binding affinity and stabilizing properties of the dye.

The direct immobilization of the dye by ligand exchange was used for the *in vivo* detection of hydroxyl radicals (Z. Li et al. 2015). The oleate was first removed from the surface of hydrophobic $NaYF_4$:Yb,Tm@$NaYF_4$ UCNPs by the addition of HCl. Subsequently, the surface of the obtained ligand free particles was passivated with a carboxyl-modified azo dye that absorbed the blue luminescence around 475 nm of the UCNPs and efficiently quenched the intensity of the affected UCNP emission. Hydroxyl radicals oxidized the azo dye, thus altering its absorption properties and preventing the energy transfer from the UCNPs. This process was monitored by the corresponding increase of the luminescence intensity of the blue UCNP emission. The colloidal stability of the nanoprobes under physiological conditions was sufficient for the successful performance of *in vivo* measurements.

If the active dye does not possess any functional groups or only weakly coordinating ones, a linker molecule can be first attached to the UCNPs by ligand replacement. This first layer can then be used to immobilize the respective dyes covalently or electrostatically. Suitable linkers in these cases are hydrophilic polymers, like PAA and poly(allyl amine) (PAAm). They simultaneously impart water dispersibility, a high surface charge for

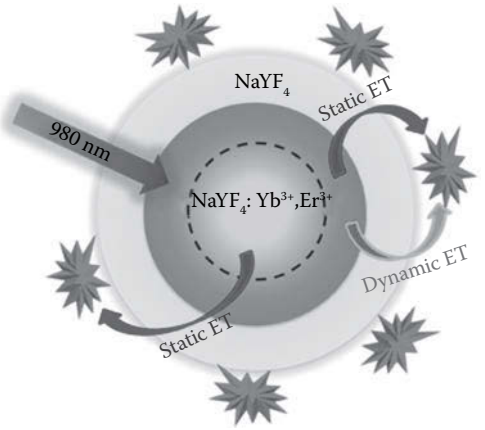

FIGURE 4.8
Energy transfer model from Er^{3+} in core–shell $NaYF_4$:Yb^{3+},Er^{3+}@$NaYF_4$ UCNPs to surface-bound acceptor rose bengal. (Reprinted with permission from Ding et al. 2015. Copyright 2015 American Chemical Society.)

electrostatic adsorption, and functional groups for covalent attachment of the dyes.

This strategy was used for the development of a UCNP nanocarrier for the photosensitizer rose bengal (Y. Ding et al. 2015). First, the oleate was exchanged with PAAm assisted by the addition of HCl. Afterwards, rose bengal was coupled to the amino groups by carbodiimide activation. Figure 4.8 shows the modified core–shell nanoparticles with the covalently bound dye molecules. The resulting system was used to determine the effect of the distance between UCNP and dye on the energy transfer efficiency.

In another example, PAA was introduced as the first polymer layer after the ligand exchange (Peng et al. 2015). A positively charged Zn^{2+} sensitive dye was adsorbed to the polymer-coated UCNPs via electrostatic interactions. In the absence of Zn^{2+} ions, the absorption of the dye nicely overlaps with the blue emission of $NaYF_4$:Yb,Tm. Increasing Zn^{2+} concentrations cause a blue shift of the dye absorption and the recovery of the UCNP emission. The modified particles were stable in cell culture media and were successfully applied for *in vivo* detection of Zn^{2+} in zebrafish.

Protease activities have also been monitored based on energy transfer between UCNPs and the fluorescent dye carboxytetramethylrhodamine (TAMRA) (Zeng et al. 2015). The C-terminus of an oligopeptide was modified with TAMRA and the peptide was immobilized on the surface of UCNPs by ligand exchange, resulting in a reduction of the luminescence intensity of the green upconversion emission. Cleavage of the peptide by trypsin and caspase-3 released the TAMRA dye from the particle surface and the emission intensity gradually increased. The particles displayed great colloidal stability when transferred into water under high peptide concentrations to

ensure sufficient surface coverage and charge. They were used for the sensitive determination of protease activities and tumor cell imaging.

Hydrophobic, not water-soluble dyes cannot be attached to the UCNPs via ligand exchange for use in bioapplications, as they do not render the particles water dispersible. One alternative is the coating of oleate-capped UCNPs with amphiphilic molecules. This technique can be used to trap small dyes (and other molecules) inside the hydrophobic bilayer. At the same time, the particles are transferred into the aqueous phase and the choice of the amphiphilic molecule provides additional possibilities for further conjugation steps. Modifications with amphiphilic molecules generally display low aggregation tendencies during the coating process and lead to excellent colloidal stability in various buffers and cell culture media.

The photosensitizer merocyanine 540 was loaded into the bilayer formed by the addition of various phospholipids (H. Wang et al. 2014) or amphiphilic polymers, such as the triblock copolymer Pluronic®F-127 (H. Ding et al. 2015) to oleate-capped UCNPs. Furthermore, the particles were decorated with targeting moieties for tumor cells. The successful entrapment of the photosensitizer within the hydrophobic bilayer was demonstrated by the efficient production of singlet oxygen upon NIR excitation of the UCNPs and energy transfer to the MC540 inside breast cancer cells.

Molecules inside the hydrophobic bilayer were shown to retain their responsive properties. For example, the methylmercury sensitive cyanine dye hCy7 was immobilized within a bilayer formed by the amphiphilic block-polymer PMAO–PEG and the oleate ligands (Y. Liu et al. 2013). In absence of methylmercury, the red emission at 660 nm of the UCNPs was quenched due to an efficient energy transfer to the dye. The addition of methylmercury induced a shift of the hCy7 absorption and the upconversion luminescence was recovered. Figure 4.9 shows the surface modification and the detection principle of the nanoparticles against $MeHg^+$. The sensor did not show cross sensitivity to numerous metal ions while methylmercury could be monitored *in vivo* with a detection limit of about 0.8 ppb.

The same group used a very similar technique to detect hypochlorite (Zou et al. 2015). They incorporated the cyanine dye hCy3 with long alkyl side chains inside the bilayer formed by an amphiphilic polymer around oleate-capped $NaYF_4$:Yb,Nd,Er@$NaYF_4$:Nd nanoparticles. The hCy3 dye was able to absorb the green emission of the UCNPs. The fluorescent dye reacted irreversibly with ClO^- leading to an increase of the luminescence intensity of the upconversion nanocrystals. Hypochlorite pretreated HeLa cells were incubated with the 808 nm excitable nanoparticles to detect the pathogen using confocal microscopy.

Aside from entrapment within the surfactant bilayer, the dyes can also be covalently attached to the hydrophilic part of the amphiphilic molecules. This is required if the dyes are too hydrophilic for efficient vdW interactions with the alkyl chains or too large for stable incorporation in the bilayer in order to prevent leakage.

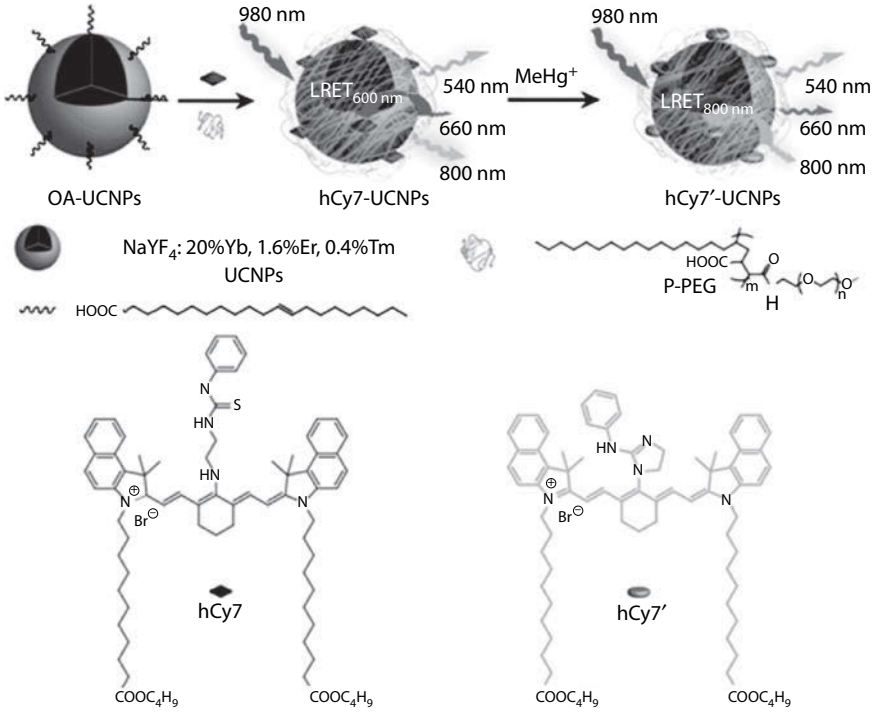

FIGURE 4.9
Schematic illustration of the synthesis of UCNPs-hCy7 and its sensing principle to $MeHg^+$ with a change in upconversion emission. (Reprinted with permission from Liu et al. 2013. Copyright 2013 American Chemical Society.)

With this strategy, UCNPs coated with both a porphyrin-functionalized phospholipid and a PEG–phospholipid suitable for multimodal imaging were obtained (Rieffel et al. 2015). Despite only two imaging components were used, the UCNP itself and the porphyrin, the particles were active in six different imaging modalities, including positron emission tomography, X-ray computed tomography, and photoacoustic imaging. This was demonstrated by *in vivo* lymphatic imaging in mice and revealed significant contrast enhancement.

High stability against leaching of the dyes from the surface of the UCNPs is provided by silica coating with subsequent covalent attachment of the dye. The conjugation can be performed by either surface silanization with silane-modified dyes or by coupling to functional groups on the silica surface.

The former method was used for the design of core–shell nanocomposites for NIR imaging and photothermal therapy (Shan et al. 2013). $NaYF_4$:Yb,Er UCNPs were encapsulated inside a silica shell by the polymerization of TEOS via the reverse microemulsion method. Secondly, the silane-modified NIR canine dye CyTE-777-triethoxysilane was covalently bound to the silica shell. These dye carrying nanoparticles were colloidally stable in water

for over 1 year. Incubation of macrophage cells with the nanocomposites enabled upconversion imaging upon excitation at 980 nm. Excitation of the organic dye loaded on the surface of the UCNPs led to efficient cell death and a cell viability of only 50% after 1 h, proving the photothermal treatment capabilities of the particles.

Functional groups can be integrated into the silica shell by the addition of functional organosilanes during the growth period of the silica shell. Amino groups were generated by the application of, for example, (N-(3-trimethoxysilyl)propyl)ethylene diamine (Arppe et al. 2014) and 3-(triethoxysilyl)propyl isocyanate (Ma et al. 2015) in the polymerization phase. Afterwards, pH-sensitive organic dyes, pHrodo™ Red and xylene orange, displaying a spectral overlap with one emission band of the UCNPs were coupled to those amino groups via EDC/NHS chemistry. The ratiometric readout of pH-induced changes in the emission intensities caused by shifts in the absorption spectra of the dyes revealed a resolution of 0.3 pH units. Furthermore, as the UCNP–dye composites were colloidally stable under physiological conditions, they were used for the imaging of intracellular pH values inside HeLa cells.

Dyes can also be directly and covalently integrated into the silica shell (Zhou et al. 2015). In one example, first a silica shell was formed around UCNPs with three different dopants by the polymerization of TEOS. Then, either aminopropyl triethoxysilane-modified rhodamine B isothiocyanate or nickel (II) phthalocyanine-tetrasulfonic acid was added and polymerized on top of the previous silica shell. This dye-containing layer served as an emission filter to generate single-band emitting UCNPs and provided dispersibility and stability in physiological buffers. This way, single green, red, and blue emitting UCNPs were obtained by filtering either the red or the green emission in Yb,Er- and Yb,Tm-doped particles, respectively, with the dye layer. The conjugation to specific antibodies was performed by coupling to the amino groups of the dye-doped silica shell. The surface engineering leading to these single-band emitting conjugates is shown in Figure 4.10. The excellent properties of the modified UCNPs were demonstrated by multiplexed imaging of cancer biomarkers.

Although intentional in the last example, the downside of the modification with a silica shell regarding energy transfer efficiency is the significant increase of the distance between the donor UCNPs and the acceptor dyes. Mesoporous or rattle-structured (J. Liu et al. 2014) silica at least partly bypasses this problem, since the attachment of the dye does not only occur at the outer surface of the silica shell, but also within the whole shell itself. This also significantly increases the loading capacity of the whole system due to a greatly enlarged surface area available for the immobilization.

Mesoporous silica ($mSiO_2$) is usually synthesized by removing the template for the porous structure after the polymerization of the silicate precursors. In a first step, the silica shell is completely formed around UCNPs coated with surfactants, such as hexadecyl trimethylammonium bromide (CTAB).

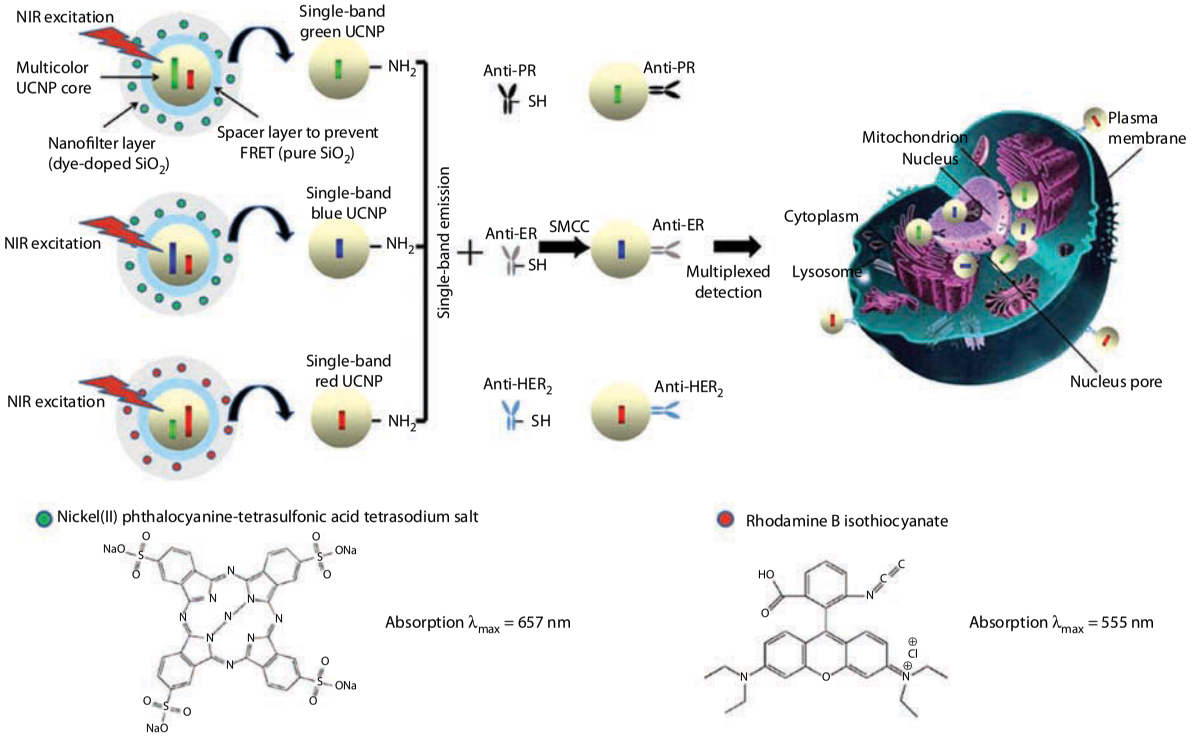

FIGURE 4.10
Surface amino modifications of the multilayer structure of green, blue, and red single-band emitting UCNPs and conjugates with antibodies for multiplexed *in situ* molecular mapping of breast cancer biomarkers. (Reprinted with permission from Zhou, L., R. Wang, C. Yao et al. 2015. Single-band upconversion nanoprobes for multiplexed simultaneous *in situ* molecular mapping of cancer biomarkers. *Nat. Commun.* 6, 6938, distributed under a Creative Commons CC-BY license.)

Subsequently, the surfactant can be removed by ion exchange, resulting in the formation of disordered, wormhole-like structures inside the silica shell (S. Liu et al. 2014). Particles covered with $mSiO_2$ displayed colloidal stability in PBS. The pores were, for example, loaded with a merocyanine (MC) dye, which is reactive against hydrogen sulfide. Its oxidized form possesses a spectral overlap with the green UCNP emission, while the reduced structure formed in presence of HS^- does not, as illustrated in Figure 4.11. This allowed

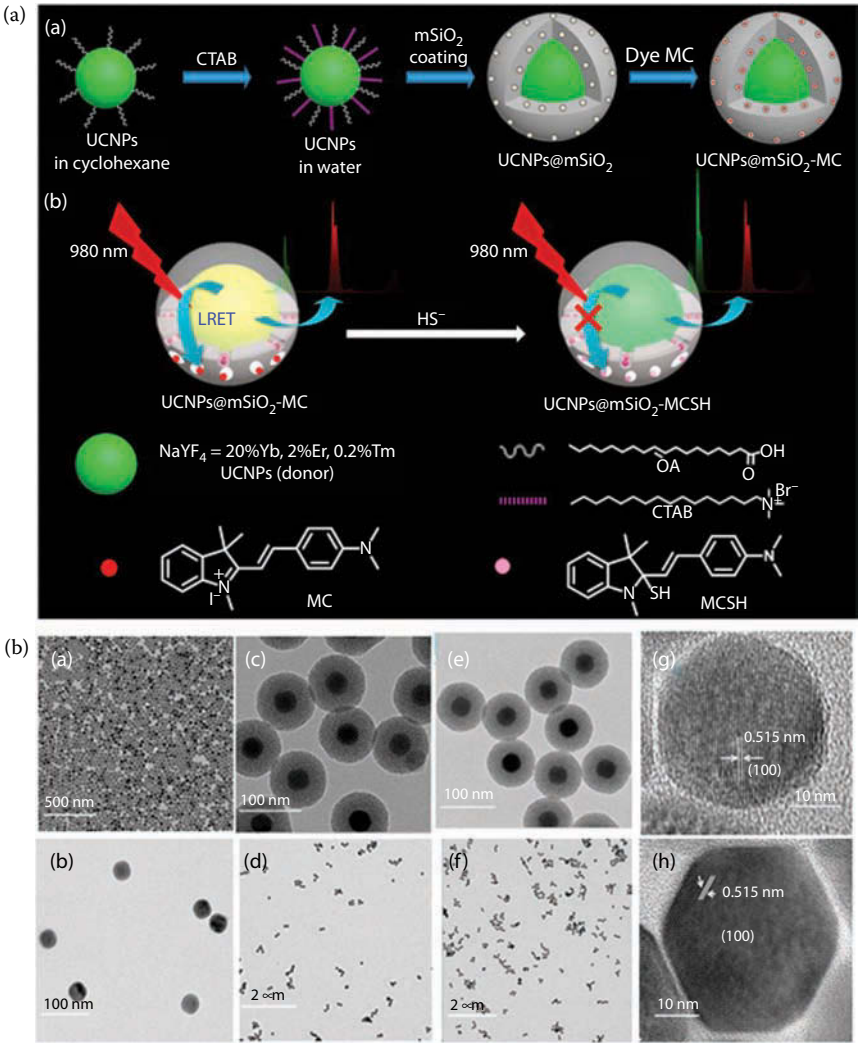

FIGURE 4.11
(a) Design strategy and synthetic route of nanoprobe UCNPs@SiO_2-MC. (b) Sensing mechanism and energy transfer process of UCNPs@SiO_2-MC toward HS^-. (Adapted with permission from Liu et al. 2014. Copyright 2014 American Chemical Society.)

the ratiometric evaluation of the luminescence intensities with a detection limit of 0.58 μM.

4.7 Conclusion

The most common surface modifications of hydrophobic UCNPs are the ligand exchange method and the encapsulation with silica to obtain water stable dispersions. For the ligand exchange strategy, PAA is the most popular hydrophilic ligand, due to its high binding affinity to the surface of the nanoparticles utilizing the chelate effect. Direct attachment of the signal molecules is also a frequently performed method requiring only functional groups capable of coordinating to the lanthanide ions on the surface. Encapsulation with inorganic silica shells creates colloidally stable particles in aqueous media. One drawback of the silica coating is the tendency for agglomeration, especially after centrifugation, which can be avoided by smart surface engineering.

The modified nanoparticles are often colloidally stable in HEPES and tris(hydroxymethyl)aminomethane (TRIS) buffer; however, they suffer from agglomeration in phosphate-buffered solutions. To achieve stability in PBS, coating with phospholipids and ligand exchange with phosphonic acid groups have proven their applicability in biological samples. For further (bio)modification, almost exclusively classical EDC chemistry or maleimide chemistry are used to bind DNA, dyes, and proteins to the surface of the particles. The overall well-established click chemistry is scarcely applied for bioconjugation of UCNPs (C. Liu et al. 2014; T. Wu et al. 2013). Very often the aspects of crosslinking and agglomeration are not further discussed. Table 4.1 gives a general overview of aspects to consider

TABLE 4.1

Suitability of Surface Modification Strategies Regarding the Final Application

Application	Surface Modification Strategy	Advantages
Sensors (via energy transfer)	Ligand exchange, mesoporous silica shell	Minimum distance between donor and acceptor
Electrophoresis	Amphiphilic polymers, silica coating	Stability against ligand detachment
Cellular imaging	Silica coating, amphiphilic polymers	Stability in cell culture media
Bioconjugation	Amphiphilic molecules, silica coating, ligand exchange	Variety of head groups available, stability in buffers
Cellular uptake	Amphiphilic polymers, silica shell	Mimicking of biological systems, tunable surface charge

when choosing the appropriate surface modification method for different applications.

One general issue of all surface modifications is the difficulty to compare individual methods and the absence of a standard for the surface characterization. The amount of surface ligands and signal molecules is often not characterized resulting in a low reproducibility of the techniques. For example, the amount of dye molecules loaded onto the surface of UCNPs nanoparticles is rarely specified or proofed. Due to the high dye loading capacities of the UCNPs, absorbance and fluorescence measurements are only conditionally suitable.

Therefore, inductively coupled plasma measurements, nuclear magnetic resonance spectroscopy, and thermogravimetric analysis should be generally established to characterize the surface of the modified UCNPs.

Despite the challenges in characterization and control of the surface properties of functionalized UCNPs, numerous bioapplications of UCNPs clearly demonstrate the outstanding advantage of almost background free measurements upon NIR excitation. Nevertheless, the strong water absorption at the typical excitation wavelength of 980 nm causes heating of biological samples and low upconversion efficiency. This drawback has recently been overcome by the design of core–shell architectures with additional Nd^{3+} ions as sensitizers, shifting the excitation wavelength to 808 nm. It is expected that this class of UCNPs will gain further interest in upconversion technologies, especially for bioanalytical applications.

Acknowledgment

We acknowledge the COST action CM1403 "The European Upconversion Network: From the Design of Photon-Upconverting Nanomaterials to Biomedical Applications."

References

Alonso-Cristobal, P., P. Vilela, A. El-Sagheer et al. 2015. Highly sensitive DNA sensor based on upconversion nanoparticles and graphene oxide. *ACS Appl. Mater. Inter.* 7:12422–12429.

Arppe, R., T. Nareoja, S. Nylund et al. 2014. Photon upconversion sensitized nanoprobes for sensing and imaging of pH. *Nanoscale* 6:6837–6843.

Bagwe, R. P., L. R. Hilliard, and W. Tan. 2006. Surface modification of silica nanoparticles to reduce aggregation and nonspecific binding. *Langmuir* 22:4357–4362.

Bogdan, N., F. Vetrone, G. A. Ozin, and J. A. Capobianco. 2011. Synthesis of ligand-free colloidally stable water dispersible brightly luminescent lanthanide-doped upconverting nanoparticles. *Nano Lett.* 11:835–840.

Boyer, J.-C., L. A. Cuccia, and J. A. Capobianco. 2007. Synthesis of colloidal upconverting $NaYF_4$: Er^{3+}/Yb^{3+} and Tm^{3+}/Yb^{3+} monodisperse nanocrystals. *Nano Lett.* 7:847–852.

Boyer, J.-C., F. Vetrone, L. A. Cuccia, and J. A. Capobianco. 2006. Synthesis of colloidal upconverting $NaYF_4$ nanocrystals doped with Er^{3+}, Yb^{3+} and Tm^{3+}, Yb^{3+} via thermal decomposition of lanthanide trifluoroacetate precursors. *J. Am. Chem. Soc.* 128:7444–7445.

Chen, G., H. Qiu, P. N. Prasad, and X. Chen. 2014. Upconversion nanoparticles: Design, nanochemistry, and applications in theranostics. *Chem. Rev.* 114:5161–5214.

Chien, Y.-H., Y.-L. Chou, S.-W. Wang et al. 2013. Near-infrared light photocontrolled targeting, bioimaging, and chemotherapy with caged upconversion nanoparticles *in vitro* and *in vivo*. *ACS Nano* 7:8516–8528.

Ding, H., Y. Lv, D. Ni et al. 2015. Erythrocyte membrane-coated NIR-triggered biomimetic nanovectors with programmed delivery for photodynamic therapy of cancer. *Nanoscale* 7:9806–9815.

Ding, Y., F. Wu, Y. Zhang et al. 2015. Interplay between static and dynamic energy transfer in biofunctional upconversion nanoplatforms. *J. Phys. Chem. Lett.* 6:2518–2523.

Dong, A., X. Ye, J. Chen et al. 2011. A generalized ligand-exchange strategy enabling sequential surface functionalization of colloidal nanocrystals. *J. Am. Chem. Soc.* 133:998–1006.

Doughan, S., Y. Han, U. Uddayasankar, and U. J. Krull. 2014. Solid-phase covalent immobilization of upconverting nanoparticles for biosensing by luminescence resonance energy transfer. *ACS Appl. Mater. Inter.* 6:14061–14068.

Gao, H.-D., P. Thanasekaran, C.-W. Chiang et al. 2015. Construction of a near-infrared-activatable enzyme platform to remotely trigger intracellular signal transduction using an upconversion nanoparticle. *ACS Nano* 9:7041–7051.

Haase, M. and H. Schäfer. 2011. Upconverting nanoparticles. *Angew. Chem. Int. Ed.* 50:5808–5829.

Huang, L.-J., X. Tian, J.-T. Yi, R.-Q. Yu, and X. Chu. 2015a. A turn-on upconversion fluorescence resonance energy transfer biosensor for ultrasensitive endonuclease detection. *Anal Methods* 7:7474–7479.

Huang, L.-J., R.-Q. Yu, and X. Chu. 2015b. DNA-functionalized upconversion nanoparticles as biosensors for rapid, sensitive, and selective detection of Hg^{2+} in complex matrices. *Analyst* 140:4987–4990.

Idris, N. M., M. K. Gnanasammandhan, J. Zhang, P. C. Ho, R. Mahendran, and Y. Zhang. 2012. *In vivo* photodynamic therapy using upconversion nanoparticles as remote-controlled nanotransducers. *Nat. Med.* 18:1580–1585.

Jalil, R. A. and Y. Zhang. 2008. Biocompatibility of silica coated $NaYF_4$ upconversion fluorescent nanocrystals. *Biomaterials* 29:4122–4128.

Jayakumar, M. K. G., N. M. Idris, K. Huang, and Y. Zhang. 2014. A paradigm shift in the excitation wavelength of upconversion nanoparticles. *Nanoscale* 6:8441–8443.

Jiang, G., J. Pichaandi, N. J. J. Johnson, R. D. Burke, and F. C. J. M. van Veggel. 2012. An effective polymer cross-linking strategy to obtain stable dispersions of upconverting $NaYF_4$ nanoparticles in buffers and biological growth media for biolabeling applications. *Langmuir* 28:3239–3247.

Johnson, N. J. J., A. Korinek, C. Dong, and F. C. J. M. van Veggel. 2012. Self-focusing by Ostwald ripening: A strategy for layer-by-layer epitaxial growth on upconverting nanocrystals. *J. Am. Chem. Soc.* 134:11068–11071.

Johnson, N. J. J., N. M. Sangeetha, J.-C. Boyer, and F. C. J. M. van Veggel. 2010. Facile ligand-exchange with polyvinylpyrrolidone and subsequent silica coating of hydrophobic upconverting β-$NaYF_4$:Yb^{3+}/Er^{3+} nanoparticles. *Nanoscale* 2:771–777.

Lan, J., F. Wen, F. Fu et al. 2015. A photoluminescent biosensor based on long-range self-assembled DNA cascades and upconversion nanoparticles for the detection of breast cancer-associated circulating microRNA in serum samples. *RSC Adv.* 5:18008–18012.

Li, C., Z. Hou, Y. Dai et al. 2013. A facile fabrication of upconversion luminescent and mesoporous core–shell structured β-$NaYF_4$: Yb^{3+} Er^{3+}@$mSiO_2$ nanocomposite spheres for anti-cancer drug delivery and cell imaging. *Biomater. Sci.* 1:213–223.

Li, K., Q. Su, W. Yuan et al. 2015. Ratiometric monitoring of intracellular drug release by an upconversion drug delivery nanosystem. *ACS Appl. Mater. Inter.* 7:12278–12286.

Li, L.-L., P. Wu, K. Hwang, and Y. Lu. 2013. An exceptionally simple strategy for DNA-functionalized up-conversion nanoparticles as biocompatible agents for nanoassembly, DNA delivery, and imaging. *J. Am. Chem. Soc.* 135:2411–2414.

Li, X., Y. Wu, Y. Liu, X. Zou, L. Yao, F. Li, and W. Feng. 2014. Cyclometallated ruthenium complex-modified upconversion nanophosphors for selective detection of Hg^{2+} ions in water. *Nanoscale* 6:1020–1028.

Li, Y., Z. Wu, and Z. Liu. 2015. An immune sandwich assay of carcinoembryonic antigen based on the joint use of upconversion phosphors and magnetic beads. *Analyst* 140:4083–4088.

Li, Z., T. Liang, S. Lv, Q. Zhuang, and Z. Liu. 2015. A rationally designed upconversion nanoprobe for *in vivo* detection of hydroxyl radical. *J. Am. Chem. Soc.* 137:11179–11185.

Liang, S., X. Zhang, Z. Wu et al. 2012. Decoration of up-converting $NaYF_4$:Yb,Er(Tm) nanoparticles with surfactant bilayer. A versatile strategy to perform oil-to-water phase transfer and subsequently surface silication. *CrystEngComm* 14:3484–3489.

Liu, C., W. Ma, Z. Gao et al. 2014. Upconversion luminescence nanoparticles-based lateral flow immunochromatographic assay for cephalexin detection. *J. Mater. Chem. C* 2:9637–9642.

Liu, F., Q. Zhao, H. You, and Z. Wang. 2013. Synthesis of stable carboxy-terminated $NaYF_4$: Yb^{3+}, Er^{3+}@SiO_2 nanoparticles with ultrathin shell for biolabeling applications. *Nanoscale* 5:1047–1053.

Liu, J., W. Bu, L. Pan, and J. Shi. 2013. NIR-triggered anticancer drug delivery by upconverting nanoparticles with integrated azobenzene-modified mesoporous silica. *Angew. Chem. Int. Ed.* 52:4375–4379.

Liu, J., Y. Liu, W. Bu et al. 2014. Ultrasensitive nanosensors based on upconversion nanoparticles for selective hypoxia imaging *in vivo* upon near-infrared excitation. *J. Am. Chem. Soc.* 136:9701–9709.

Liu, S., L. Zhang, T. Yang et al. 2014. Development of upconversion luminescent probe for ratiometric sensing and bioimaging of hydrogen sulfide. *ACS Appl. Mater. Inter.* 6:11013–11017.

Liu, Y., M. Chen, T. Cao et al. 2013. A cyanine-modified nanosystem for *in vivo* upconversion luminescence bioimaging of methylmercury. *J. Am. Chem. Soc.* 135:9869–9876.

Lu, S., D. Tu, P. Hu et al. 2015. Multifunctional nano-bioprobes based on rattle-structured upconverting luminescent nanoparticles. *Angew. Chem. Int. Ed.* 54:7915–7919.

Ma, C., T. Bian, S. Yang et al. 2014. Fabrication of versatile cyclodextrin-functionalized upconversion luminescence nanoplatform for biomedical imaging. *Anal. Chem.* 86:6508–6515.

Ma, T., Y. Ma, S. Liu et al. 2015. Dye-conjugated upconversion nanoparticles for ratiometric imaging of intracellular pH values. *J. Mater. Chem. C* 3:6616–6620.

Min, Y., J. Li, F. Liu, E. K. Yeow, and B. Xing. 2014. Near-infrared light-mediated photoactivation of a platinum antitumor prodrug and simultaneous cellular apoptosis imaging by upconversion luminescent nanoparticles. *Angew. Chem. Int. Ed.* 53:1012–1016.

Muhr, V., S. Wilhelm, T. Hirsch, and O. S. Wolfbeis. 2014. Upconversion nanoparticles: From hydrophobic to hydrophilic surfaces. *Acc. Chem. Res.* 47:3481–3493.

Nam, S. H., Y. M. Bae, Y. I. Park et al. 2011. Long-term real-time tracking of lanthanide ion doped upconverting nanoparticles in living cells. *Angew. Chem.* 123:6217–6221.

Ni, D., J. Zhang, W. Bu et al. 2014. Dual-targeting upconversion nanoprobes across the blood-brain barrier for magnetic resonance/fluorescence imaging of intracranial glioblastoma. *ACS Nano* 8:1231–1242.

Ong, L. C., L. Y. Ang, S. Alonso, and Y. Zhang. 2014. Bacterial imaging with photostable upconversion fluorescent nanoparticles. *Biomaterials* 35:2987–2998.

Park, Y. I., J. H. Kim, K. T. Lee et al. 2009. Nonblinking and nonbleaching upconverting nanoparticles as an optical imaging nanoprobe and T1 magnetic resonance imaging contrast agent. *Adv. Mater.* 21:4467–4471.

Pellegrino, T., L. Manna, S. Kudera et al. 2004. Hydrophobic nanocrystals coated with an amphiphilic polymer shell: A general route to water soluble nanocrystals. *Nano Lett.* 4:703–707.

Peng, J., W. Xu, C. L. Teoh et al. 2015. High-efficiency *in vitro* and *in vivo* detection of Zn^{2+} by dye-assembled upconversion nanoparticles. *J. Am. Chem. Soc.* 137:2336–2342.

Qiao, R., C. Liu, M. Liu et al. 2015. Ultrasensitive *in vivo* detection of primary gastric tumor and lymphatic metastasis using upconversion nanoparticles. *ACS Nano* 9:2120–2129.

Ren, W., G. Tian, S. Jian et al. 2012. TWEEN coated $NaYF_4$:Yb,Er/$NaYF_4$ core/shell upconversion nanoparticles for bioimaging and drug delivery. *RSC Adv.* 2:7037–7041.

Rieffel, J., F. Chen, J. Kim et al. 2015. Hexamodal imaging with porphyrin–phospholipid-coated upconversion nanoparticles. *Adv. Mater.* 27:1785–1790.

Rinkel, T., J. Nordmann, A. N. Raj, and M. Haase. 2014. Ostwald-ripening and particle size focusing of sub-10 nm $NaYF_4$ upconversion nanocrystals. *Nanoscale* 6:14523–14530.

Shan, G., R. Weissleder, and S. A. Hilderbrand. 2013. Upconverting organic dye doped core–shell nano-composites for dual-modality NIR imaging and photothermal therapy. *Theranostics* 3:267–274.

Song, K., X. Kong, X. Liu et al. 2012. Aptamer optical biosensor without bio-breakage using upconversion nanoparticles as donors. *Chem. Commun.* 48:1156–1158.

Suyver, J. F., J. Grimm, M. K. van Veen, D. Biner, K. W. Krämer, and H. U. Güdel. 2006. Upconversion spectroscopy and properties of $NaYF_4$ doped with Er^{3+}, Tm^{3+} and/or Yb^{3+}. *J. Lumin.* 117:1–12.

Tong, L., E. Lu, J. Pichaandi, P. Cao, M. Nitz, and M. A. Winnik. 2015. Quantification of surface ligands on $NaYF_4$ nanoparticles by three independent analytical techniques. *Chem. Mater.* 27:4899–4910.

Wang, C., L. Cheng, Y. Liu et al. 2013. Imaging-guided pH-sensitive photodynamic therapy using charge reversible upconversion nanoparticles under near-infrared light. *Adv. Funct. Mater.* 23:3077–3086.

Wang, C., H. Tao, L. Cheng, and Z. Liu. 2011. Near-infrared light induced *in vivo* photodynamic therapy of cancer based on upconversion nanoparticles. *Biomaterials* 32:6145–6154.

Wang, F. and X. Liu. 2009. Recent advances in the chemistry of lanthanide-doped upconversion nanocrystals. *Chem. Soc. Rev.* 38:976–989.

Wang, F. and X. Liu. 2014. Multicolor tuning of lanthanide-doped nanoparticles by single wavelength excitation. *Acc. Chem. Res.* 47:1378–1385.

Wang, F., J. Wang, and X. Liu. 2010. Direct evidence of a surface quenching effect on size-dependent luminescence of upconversion nanoparticles. *Angew. Chem. Int. Ed.* 49:7456–7460.

Wang, H., Z. Liu, S. Wang et al. 2014. MC540 and upconverting nanocrystal coloaded polymeric liposome for near-infrared light-triggered photodynamic therapy and cell fluorescent imaging. *ACS Appl. Mater. Inter.* 6:3219–3225.

Wang, J., T. Wei, X. Li et al. 2014. Near-infrared-light-mediated imaging of latent fingerprints based on molecular recognition. *Angew. Chem.* 126:1642–1646.

Wang, L., W. Qin, Z. Liu et al. 2012. Improved 800 nm emission of Tm^{3+} sensitized by Yb^{3+} and Ho^{3+} in β-$NaYF_4$ nanocrystals under 980 nm excitation. *Opt. Express* 20:7602.

Wang, M., C.-C. Mi, W.-X. Wang et al. 2009a. Immunolabeling and NIR-excited fluorescent imaging of HeLa cells by using $NaYF_4$:Yb,Er upconversion nanoparticles. *ACS Nano* 3:1580–1586.

Wang, M., C. Mi, Y. Zhang, J. Liu, F. Li, C. Mao, and S. Xu. 2009b. NIR-responsive silica-coated $NaYbF_4$:Er/Tm/Ho upconversion fluorescent nanoparticles with tunable emission colors and their applications in immunolabeling and fluorescent imaging of cancer cells. *J. Phys. Chem. C* 113:19021–19027.

Wang, Y.-F., G.-Y. Liu, L.-D. Sun, J.-W. Xiao, J.-C. Zhou, and C.-H. Yan. 2013. Nd^{3+}-sensitized upconversion nanophosphors: Efficient *in vivo* bioimaging probes with minimized heating effect. *ACS Nano* 7:7200–7206.

Wang, Z., X. Li, Y. Song, L. Li, W. Shi, and H. Ma. 2015. An upconversion luminescence nanoprobe for the ultrasensitive detection of hyaluronidase. *Anal. Chem.* 87:5816–5823.

Wilhelm, S., M. Barrio, J. Heiland et al. 2014. Spectrally matched upconverting luminescent nanoparticles for monitoring enzymatic reactions. *ACS Appl. Mater. Inter.* 6:15427–15433.

Wilhelm, S., T. Hirsch, W. M. Patterson, E. Scheucher, T. Mayr, and O. S. Wolfbeis. 2013. Multicolor upconversion nanoparticles for protein conjugation. *Theranostics* 3:239–248.

Wilhelm, S., M. Kaiser, C. Würth et al. 2015. Water dispersible upconverting nanoparticles: Effects of surface modification on their luminescence and colloidal stability. *Nanoscale* 7:1403–1410.

Wu, S., N. Duan, X. Ma, Y. Xia, H. Wang, and Z. Wang. 2013. A highly sensitive fluorescence resonance energy transfer aptasensor for staphylococcal enterotoxin B detection based on exonuclease-catalyzed target recycling strategy. *Anal. Chim. Acta* 782:59–66.

Wu, S., N. Duan, Z. Shi, C. Fang, and Z. Wang. 2014. Simultaneous aptasensor for multiplex pathogenic bacteria detection based on multicolor upconversion nanoparticles labels. *Anal. Chem.* 86:3100–3107.

Wu, T., M. Barker, K. M. Arafeh, J.-C. Boyer, C.-J. Carling, and N. R. Branda. 2013. A UV-blocking polymer shell prevents one-photon photoreactions while allowing multi-photon processes in encapsulated upconverting nanoparticles. *Angew. Chem. Int. Ed.* 52:11106–11109.

Wu, Y.-M., Y. Cen, L.-J. Huang, R.-Q. Yu, and X. Chu. 2014. Upconversion fluorescence resonance energy transfer biosensor for sensitive detection of human immunodeficiency virus antibodies in human serum. *Chem. Commun.* 50 4759–4762.

Zeng, T., T. Zhang, W. Wei et al. 2015. Compact, programmable, and stable biofunctionalized upconversion nanoparticles prepared through peptide-mediated phase transfer for high-sensitive protease sensing and *in vivo* apoptosis imaging. *ACS Appl. Mater. Inter.* 7:11849–11856.

Zhang, F. 2014. *Photon Upconversion Nanomaterials. Nan Sci Tec*., Springer, New York.

Zhang, P., W. Steelant, M. Kumar, and M. Scholfield. 2007. Versatile photosensitizers for photodynamic therapy at infrared excitation. *J. Am. Chem. Soc.* 129:4526–4527.

Zhao, G., L. Tong, P. Cao, M. Nitz, and M. A. Winnik. 2014. Functional PEG–PAMAM-tetraphosphonate capped $NaLnF_4$ nanoparticles and their colloidal stability in phosphate buffer. *Langmuir* 30:6980–6989.

Zhou, F., M. O. Noor, and U. J. Krull. 2014. Luminescence resonance energy transfer-based nucleic acid hybridization assay on cellulose paper with upconverting phosphor as donors. *Anal. Chem.* 86:2719–2726.

Zhou, J., Z. Liu, and F. Li. 2012. Upconversion nanophosphors for small-animal imaging. *Chem. Soc. Rev.* 41:1323–1349.

Zhou, L., R. Wang, C. Yao et al. 2015. Single-band upconversion nanoprobes for multiplexed simultaneous *in situ* molecular mapping of cancer biomarkers. *Nat. Commun.* 6:6938.

Zou, X., Y. Liu, X. Zhu et al. 2015. An Nd^{3+} sensitized upconversion nanophosphor modified with a cyanine dye for the ratiometric upconversion luminescence bioimaging of hypochlorite. *Nanoscale* 7:4105–4113.